

## Large unidirectional magnetoresistance in metallic heterostructures in the spin transfer torque regime

Ting-Yu Chang <sup>1</sup>, Chih-Lin Cheng,<sup>1</sup> Chao-Chung Huang,<sup>1</sup> Cheng-Wei Peng,<sup>1</sup> Yu-Hao Huang,<sup>1</sup> Tian-Yue Chen,<sup>1</sup> Yan-Ting Liu <sup>1,\*</sup>, and Chi-Feng Pai <sup>1,2,†</sup>

<sup>1</sup>Department of Materials Science and Engineering, National Taiwan University, Taipei 10617, Taiwan

<sup>2</sup>Center of Atomic Initiative for New Materials, National Taiwan University, Taipei 10617, Taiwan



(Received 29 April 2021; revised 7 July 2021; accepted 14 July 2021; published 27 July 2021)

A large unidirectional magnetoresistance (UMR) ratio of  $UMR/R_{xx} \approx 0.36\%$  is found in W/CoFeB metallic bilayer heterostructures at room temperature. Three different regimes in terms of the current dependence of the UMR ratio are identified: a spin-dependent-scattering mechanism regime at small current densities  $J \approx 10^9$  A/m<sup>2</sup> (UMR ratio  $\propto J$ ), a spin-magnon-interaction mechanism regime at intermediate  $J \approx 10^{10}$  A/m<sup>2</sup> (UMR ratio  $\propto J^3$ ), and a spin transfer torque (STT) regime at  $J \approx 10^{11}$  A/m<sup>2</sup> (UMR ratio independent of  $J$ ). We verify the direct correlation between this large UMR and the transfer of spin angular momentum from the W layer to the CoFeB layer by both field-dependent and current-dependent UMR characterizations. Numerical simulations further confirm that the large STT-UMR stems from the tilting of the magnetization affected by the spin Hall effect-induced STTs. An alternative approach to estimate dampinglike spin torque efficiencies from magnetic heterostructures is also proposed.

DOI: [10.1103/PhysRevB.104.024432](https://doi.org/10.1103/PhysRevB.104.024432)

### I. INTRODUCTION

Magnetoresistance (MR) is one of the key physical properties to understand spin-dependent transport mechanisms in various condensed matter systems. The discovery of giant MR (GMR) [1–3] in ferromagnetic-normal metal (FM/NM) multilayer structures as well as giant tunneling MR in MgO-based magnetic tunnel junctions [4–6] further revolutionized the hard disk drive and magnetic memory technologies, respectively. More recently, the spin Hall effect (SHE) [7–9] in magnetic heterostructures with strong spin-orbit interactions is also found to give rise to novel MRs, namely, the spin Hall MR (SMR) [10–12] and the unidirectional SMR (USMR) [13–16]. These MR effects can not only be utilized to quantify charge-to-spin conversion efficiencies in various types of NM/FM magnetic heterostructures but also serve as alternate readouts for emergent magnetoresistive memory devices. From the origin point of view, the theoretical framework for SMR is more well established, in which the MR stems from the absorption or the reflection of the SHE-induced spin current at the NM/FM interface and thereby affecting the longitudinal resistance of the heterostructure via the inverse SHE (ISHE) [10,17]. Typical longitudinal SMR ratio ranges from  $\Delta\rho_{xx}/\rho_{xx}$  (or  $\Delta R_{xx}/R_{xx}$ )  $\approx 0.001$  to 1.3% [10–12]. In contrast, a solid theoretical model for USMR or UMR is still lacking, although its origin is typically attributed to an interfacial spin-dependent scattering scenario (like the GMR case [1,2]), with typical UMR ratio ranges from  $\sim 0.0019$  to 1.1% [13,14,16,18]. It was later found that the UMR in

NM/FM heterostructures consists of two major components: a spin-dependent scattering contribution (could be of bulk and/or interfacial origins) [13,14,16] and an electron-magnon scattering contribution [19–21], as respectively illustrated in Figs. 1(a) and 1(b).

In this paper, we disentangle the underlying mechanisms of the UMR in NM/FM (W/CoFeB) magnetic heterostructures by systematic current- and field-dependent MR measurements at room temperature. A broad range of current densities are applied, ranging from  $\sim 10^9$  A/m<sup>2</sup> [alternating current (AC) signal] to  $\sim 10^{11}$  A/m<sup>2</sup> [direct current (DC) signal]. A third regime of the UMR is found to be directly related to the dampinglike spin torque (DL-ST) efficiency  $\xi_{DL}$  of the magnetic heterostructures, which is like the SMR case [11,12,22]. The UMR of W/CoFeB heterostructures first increases linearly and then nonlinearly to the applied current density  $J$  as  $J$  reaches  $\sim 5 \times 10^{10}$  A/m<sup>2</sup>, which corresponds to a later defined inflection current density  $J_{\text{inflection}}$ . The UMR of W/CoFeB further saturates at a UMR ratio of  $\sim 0.36\%$  as  $J$  reaches  $\sim 10^{11}$  A/m<sup>2</sup>. By performing macrospin and micromagnetic simulations, the current-induced STs from the SHE of the NM layer are confirmed to cause the tilting of the FM magnetization, thereby creating a change in MR. Consequently, we define this additional UMR as the spin transfer torque UMR (STT-UMR), as illustrated in Fig. 1(c). Meanwhile,  $\xi_{DL}$  of the tested heterostructures can be roughly estimated by using both the experimental UMR data and the simulation results.

### II. MATERIALS SYSTEM

A series of W( $t_W$ )/Co<sub>40</sub>Fe<sub>40</sub>B<sub>20</sub>(2)/MgO(1)/Ta(2) ( $t_W$  is the thickness of the W layer, and numbers in parentheses

\*f07527076@ntu.edu.tw

†cfpai@ntu.edu.tw

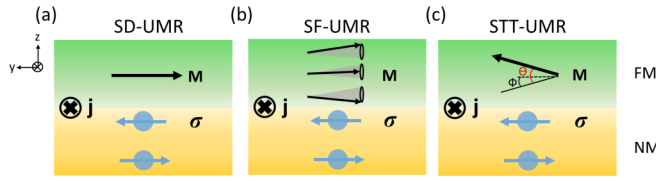


FIG. 1. Illustration of (a) spin-dependent unidirectional magnetoresistance (SD-UMR), (b) spin-flip UMR (SF-UMR), and (c) spin transfer torque UMR (STT-UMR).

are in nanometers) multilayer heterostructures were deposited onto Si/SiO<sub>2</sub> substrates by high-vacuum magnetron sputtering (base pressure  $\sim 10^{-8}$  Torr) with working Ar pressures of 3 mTorr (10 mTorr) for DC (radio frequency) sputtering. The thickness of the W layer ranged from  $t_W = 2$  to 7 nm. The top Ta layer served as a capping layer to prevent other layers from oxidation [23]. Here, all samples showed in-plane magnetic anisotropy. Saturation magnetization of the CoFeB layer was  $M_s \approx 700$  emu/cm<sup>3</sup>, as characterized by vibrating sample magnetometer. Additionally, the thickness of the magnetic dead layer was negligible in these as-deposited films [24]. To perform MR measurements, thin films were patterned into micron-sized Hall bar devices with channel width of 5  $\mu$ m through photolithography and liftoff processes.

### III. ORIGINS OF THE UMR

As shown in Fig. 2(a), to measure longitudinal resistance ( $R_{xx}$ ) on Hall bar devices, we swept the in-plane magnetic fields along the  $y$  direction ( $H_y$ ) while applying DC (opposite pulsed currents with 0.5 s duration) or AC (frequency

$\omega/2\pi = 83$  Hz) along the  $x$  direction [13,24]. We used a source meter (Keithley 2400) and a lock-in amplifier (Signal Recovery 7265) to supply DC and AC, respectively. As preliminary tests, we swept the in-plane magnetic fields within a smaller field range ( $H_{y,\max} = \pm 600$  Oe). Representative normalized UMR loops of W(4)/Co<sub>40</sub>Fe<sub>40</sub>B<sub>20</sub>(2) with AC (amplitude)  $I_{\text{sense}} = 0.079$  mA and DC ( $I_{\text{sense}} = \pm 1$  mA) are shown in Figs. 2(b) and Fig. 2(c), respectively. For the DC measurement, we recorded the difference of longitudinal resistance  $\Delta R = R_{xx}^+ - R_{xx}^-$  for applying opposite directions of DC. Note that the protocol for the DC measurement was equivalent to the Fourier-transformed second harmonic ( $2\omega$ ) signals in the AC measurement. We define the UMR as  $|(R_{H+}^{I+} - R_{H+}^{I-}) - (R_{H-}^{I+} - R_{H-}^{I-})|/2$  and  $|R_{2\omega}^{H+} - R_{2\omega}^{H-}|$  for DC and AC measurements, respectively [13,24,25]. From these experimental results, we observe that the UMR measured by DC is much larger than that by an AC, suggesting an influence of the applied current magnitude in the UMR.

Subsequently, to examine the current-dependence of the UMR, different amplitudes of DC and AC were applied to the W(4)/CoFeB(2) sample. The DC and AC current amplitudes are collectively called *sense currents* ( $I_{\text{sense}}$ ) in this section. As shown in Fig. 2(d), the UMR ratio (UMR/ $R_{xx}$ ) with applying AC is linear to  $I_{\text{sense}}$ , which is consistent with previous reports in such a low current density regime [13,16,26]. Here, UMR/ $R_{xx}$  from both DC and AC measurements are shown together in Fig. 2(e), which can be roughly divided into three regimes: In the first regime with a lower  $I_{\text{sense}}$ , UMR/ $R_{xx}$  increases linearly. In the second and the third regimes, UMR/ $R_{xx}$  rises rapidly (nonlinearly) and reaches a saturated value ( $\sim 0.36\%$ ) with increasing  $I_{\text{sense}}$ .

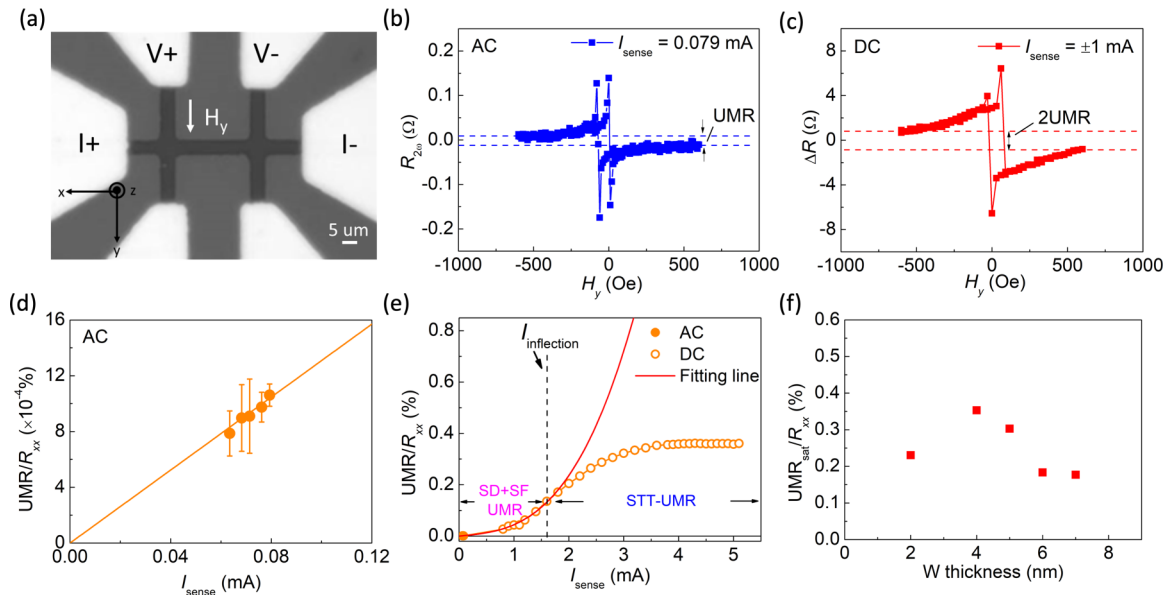


FIG. 2. (a) Optical microscopic (OM) image of a W/CoFeB Hall bar device for unidirectional magnetoresistance (UMR) measurement, which is performed by applying either alternating current (AC) or direct current (DC). Representative UMR loops as functions of in-plane field  $H_y$  with (b) an AC (amplitude)  $I_{\text{sense}} = 0.079$  mA and (c) DC ( $I_{\text{sense}} = \pm 1$  mA) for a W(4)/CoFeB(2) sample. (d) UMR/ $R_{xx}$  vs  $I_{\text{sense}}$  of a W(4)/CoFeB(2) device measured by AC with  $H_{y,\max} = \pm 600$  Oe. The solid line represents a linear fit to the experimental data. (e) Whole range  $I_{\text{sense}}$  dependence of UMR/ $R_{xx}$  with  $H_{y,\max} = \pm 600$  Oe for a W(4)/CoFeB(2) sample. The red solid line is a fit to  $(a + b)I + cI^3$  for data up to the inflection current  $I_{\text{inflection}}$ . (f) UMR/ $R_{xx}$  of W( $t_W$ )/CoFeB(2) samples as a function of W thickness ( $t_W$ ) with  $H_{y,\max} = \pm 600$  Oe.

TABLE I. Comparison of the UMR magnitude from different materials systems.

Materials system	$J$ (A/m <sup>2</sup> )	UMR ratio (%) (maximum)	Field range (T)	Reference
W/CoFeB (RT)	$1.67 \times 10^{11}$	0.36	0.06	This paper
W/CoFeB (RT)	$1.67 \times 10^{11}$	0.1	0.5	This paper
W/Co (RT)	$10^{11}$	0.0019	1.7	[14]
Co/Pt(RT)	$5 \times 10^{11}$	0.035	0.025	[16]
Ta/Co (RT)	$1.2 \times 10^{11}$	0.004	>1	[14]
GaMnAs/BiSb (30 K)	$1.5 \times 10^{10}$	1.1	0.2	[26]
CBST/BST (4 K)	$1.5 \times 10^8$	0.68	0.7	[18]

As previous works reported, conventional UMR can be separated into two major components, namely, the spin-dependent UMR (SD-UMR) and the spin-flip UMR (SF-UMR) [16,26]. These two types of UMR come from two different competing mechanisms: The SD-UMR originated from spin-dependent scattering at a large field and low current regime, while the SF-UMR is attributed to electron-magnon scattering at a low field and large current regime. Since the spin-dependent-scattering mechanism is only related to the amount of spin accumulation at the NM/FM interface and the orientation of FM magnetization  $\mathbf{M}$  with respect to the  $y$  direction [Fig. 1(a)] [13–15], SD-UMR is proportional to the magnitude of the applied current and independent of the external field, which can be described as  $aI$  ( $a$  is a field-independent coefficient). For the SF-UMR resulting from electron-magnon scattering [Fig. 1(b)], the variation of thermal-induced and spin-current-induced magnons causes the nonlinear current-dependent behavior of the UMR, which shows a  $bI + cI^3$  trend with the magnetic field-dependent coefficients  $b$  and  $c$  [16,26–30].

As shown in Fig. 2(e), the UMR/ $R_{xx}$  of the W(4)/CoFeB(2) sample ranging from 0.06 to 1.2 mA (corresponds to current densities  $J = 2.1 \times 10^9$  to  $4.0 \times 10^{10}$  A/m<sup>2</sup>) is in agreement with the trend of  $(a + b)I + cI^3$ , which suggests the behavior of the UMR can be explained by those mechanisms mentioned above. Followed by the fitting line, we can further separate this part of UMR/ $R_{xx}$  into two regimes: At small  $I_{\text{sense}}$  measured by applying AC, UMR/ $R_{xx}$  is linearly proportional to  $I_{\text{sense}}$  [Fig. 2(d)], which comes from the SD-UMR. After that, it increases nonlinearly with the increase of  $I_{\text{sense}}$  due to the SF-UMR. However, as  $I_{\text{sense}}$  becomes  $>1.2$  mA ( $J = 4.0 \times 10^{10}$  A/m<sup>2</sup>), the trend of UMR vs  $I_{\text{sense}}$  deviates from both the SD-UMR and the SF-UMR trends, suggesting an additional mechanism emerging at the high current regime. Additionally,  $I_{\text{sense}}$  vs UMR/ $R_{xx}$  is found to have an inflection point at  $I_{\text{sense}} = 1.6$  mA, signaling that the dominating mechanism has changed near this point, and we define this current as  $I_{\text{inflection}}$  ( $J_{\text{inflection}} \approx 5.0 \times 10^{10}$  A/m<sup>2</sup>).

To further gain insight into this additional UMR contribution, we measure UMR<sub>sat</sub>/ $R_{xx}$  in a series of W( $t_W$ )/CoFeB(2) samples with  $H_{y,\text{max}} = \pm 600$  Oe. As shown in Fig. 2(f), we observe that UMR<sub>sat</sub>/ $R_{xx}$  reaches a maximum ( $\sim 0.36\%$ ) at  $t_W = 4$  nm and then proceeds to decrease as further increasing  $t_W$ , which is like the trend of DL-ST efficiency  $\xi_{\text{DL}}$  vs  $W$  thickness due to the phase transition from amorphous W to  $\alpha$ -W with increasing  $t_W$  [22,31–33]. Note that  $\xi_{\text{DL}}$  is related to the internal spin Hall ratio (spin Hall angle)  $\theta_{\text{SH}}$  of the NM layer through  $\xi_{\text{DL}} = \theta_{\text{SH}} T_{\text{int}}$ , which describes the apparent ef-

iciency of the charge-to-spin conversion. Here,  $T_{\text{int}}$  is the spin transparency of the NM/FM interface [34]. Consequently, we believe that this additional UMR is related to the SHE-induced ST transfer from the heavy metal W layer into the CoFeB layer, and we tentatively define this extra UMR as the STT-UMR. It is worth noting that the anomalous Nernst effect and the spin Seebeck effect can also give rise to a similar longitudinal resistance. Nevertheless, such a thermal-induced signal is typically  $\sim 1$  m $\Omega$  in metallic systems [13,15,35], which is three orders of magnitude smaller than the UMR observed in the STT-dominated regime in our samples, therefore resulting in a comparably negligible thermal contribution.

In Table I, we compare the maximum UMR ratio of our W/CoFeB heterostructures with different materials systems previously reported. Since the maximum UMR ratio in this paper is independent of the applied current at the large current regime, we take other groups' UMR ratios under the largest current applied for a fair comparison. Note that, although the maximum UMR ratio for the W/CoFeB heterostructure is only slightly smaller than those for GaMnAs/BiSb and  $\text{Cr}_x(\text{Bi}_{1-y}\text{Sb}_y)_{2-x}\text{Te}_3/(\text{Bi}_{1-y}\text{Sb}_y)_2\text{Te}_3$  (CBST/BST) heterostructures involving topological insulators (under cryogenic condition), it can be detected at room temperature and is much larger than those observed in other NM/FM bilayer systems, e.g., W/Co or Pt/Co [13,14,16,18,26], potentially due to a more pronounced ST contribution. Another DC-induced MR effect has also been observed in  $\text{Ga}_{0.91}\text{Mn}_{0.09}\text{As}/\text{Ga}_{0.97}\text{Mn}_{0.03}\text{As}$  bilayer system, which is coined as the linear SMR (LSMR) [25]. However, since the LSMR mainly comes from the thermal effect in such a semiconductor system, it is not included here for comparison.

#### IV. CURRENT- AND FIELD-DEPENDENT UMR

We further performed field-dependent UMR measurements with a wider field range (up to 5 k Oe) while applying various  $I_{\text{sense}}$  to investigate the possible origins of such STT-UMR. As shown in Fig. 3(a), for a W(4)/CoFeB(2) sample, the trend of field-dependent UMR/ $R_{xx}$  with  $I_{\text{sense}} = 0.8$  mA ( $J = 2.7 \times 10^{10}$  A/m<sup>2</sup>) follows the fitting line of  $H_y^{-p}$  with the exponent  $p = 1.37$ , which indicates that the UMR/ $R_{xx}$  at small current densities is indeed governed by the SF-UMR [16]. With the increase of  $I_{\text{sense}}$ , the effect of ST begins to emerge, and the field-dependent UMR/ $R_{xx}$  no longer follows  $H_y^{-p}$ . Since the SF-UMR are suppressed by the ST, the relative SF-UMR contribution decreases, causing the deviation of the field-dependent UMR/ $R_{xx}$  from the trend of  $H_y^{-p}$ . For  $I_{\text{sense}} = 1.6$  mA ( $J = 5.4 \times 10^{10}$  A/m<sup>2</sup>), the

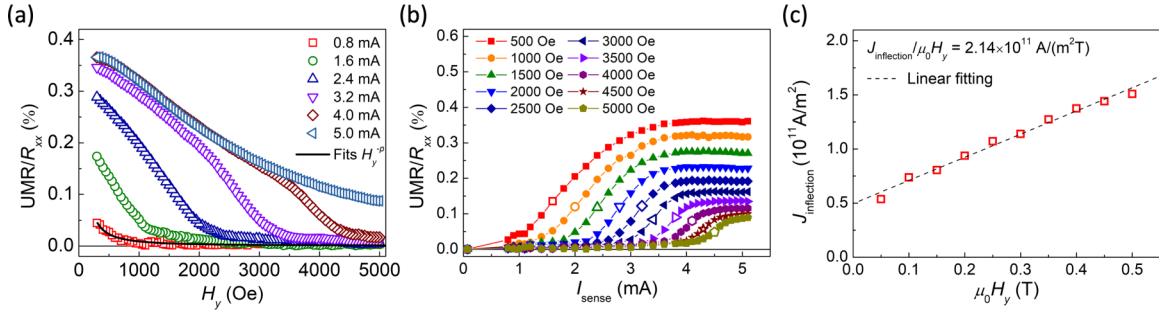


FIG. 3. (a) Field-dependent unidirectional magnetoresistance (UMR)/ $R_{xx}$  of a W(4)/CoFeB(2) sample with various  $I_{\text{sense}}$ . The solid line represents a fit to the experimental data of  $I_{\text{sense}} = 0.8$  mA with the exponent  $p = 1.37$ . (b) Current-dependent UMR/ $R_{xx}$  with different  $H_y$ . The open dots in each set of data represent  $I_{\text{inflection}}$  under different  $H_y$ . (c)  $\mu_0 H_y$  dependence of  $J_{\text{inflection}}$  extracted from (b). The dashed line is a linear fit to the data.

field-dependent UMR/ $R_{xx}$  shows a linear trend at the low field regime, suggesting that the competition between the SF- and the STT-UMR has begun. As  $I_{\text{sense}}$  gets even larger, STT-UMR becomes the dominating mechanism of the measured UMR, and the UMR ratio remains fairly constant ( $\sim 0.36\%$ ) at the low  $H_y$  regime. However, regardless of  $I_{\text{sense}}$ , the STT-UMR will eventually be canceled out at a sufficiently large  $H_y$ , indicating that the current-induced ST or its effective field is suppressed by  $H_y$ .

As an alternative way to demonstrate this effect, we measured UMR/ $R_{xx}$  vs  $I_{\text{sense}}$  with various  $H_y$ . As shown in Fig. 3(b), there are two major features: First, the saturated UMR<sub>sat</sub>/ $R_{xx}$  decreases from 0.36 to 0.09% with the increase of  $H_y$ . Second,  $I_{\text{inflection}}$  becomes larger as  $H_y$  increases, which suggests that a larger ST is required to overcome the increase of  $H_y$ . Based on the field- and the current-dependent UMR/ $R_{xx}$ , we find that both trends are in disagreement with the fitting curves at the low field ( $H_y^{-p}$ ) and in the high current regime [ $(a+b)I + cI^3$ ]. These results suggest that SF-UMR no longer governs UMR/ $R_{xx}$ , and STT-UMR dominates UMR/ $R_{xx}$  in the high current regime.

In Fig. 3(c), we summarize the  $H_y$  dependence of the inflection current density  $J_{\text{inflection}}$ , where a linear trend is found with a slope of  $J_{\text{inflection}}/\mu_0 H_y \approx 2.14 \times 10^{11}$  A/(m<sup>2</sup>T). These features again indicate that the extra UMR is a result of the competition between ST and  $H_y$  since  $H_y$  aligns  $\mathbf{M}$  toward the  $y$  direction, whereas  $\mathbf{M}$  can also be tilted toward the  $x$  and  $z$  directions by applying a countering ST. Therefore, we further suspect that this additional UMR originated from the SMR ( $\propto 1 - m_x^2$ ) and/or anisotropic MR (AMR,  $\propto m_x^2$ ) caused by the ST-induced tilting of  $\mathbf{M}$  [13] in the heterostructure [Fig. 1(c)].

## V. NUMERICAL SIMULATIONS

To confirm that STT-UMR can be attributed to the extra SMR and/or AMR contributions due to the competition between ST and  $H_y$ , we performed macrospin simulations to investigate the influence of current-induced STs [both DL and fieldlike (FL)] and applied fields on the magnetization  $\mathbf{M} = (m_x, m_y, m_z)$ . The macrospin simulations are based on the Landau-Lifshitz-Gilbert (LLG) equation with additional ST terms:

$$\frac{d\mathbf{m}}{dt} = -\gamma \mathbf{m} \times \mathbf{H}_{\text{eff}} + \alpha \mathbf{m} \times \frac{d\mathbf{m}}{dt} + \gamma H_{\text{DL}} \mathbf{m} \times (\boldsymbol{\sigma} \mathbf{m}) + \gamma H_{\text{FL}} (\boldsymbol{\sigma} \times \mathbf{m}), \quad (1)$$

where  $\mathbf{H}_{\text{eff}}$  is effective field composed of external field and anisotropy field,  $\gamma$  is the gyromagnetic ratio,  $\alpha$  is the Gilbert damping constant,  $H_{\text{DL}}$  and  $H_{\text{FL}}$  are the effective fields originated from the current-induced DL-ST and FL-ST generated by the SHE in the heavy metal layer. We considered both effective fields proportional to the applied current density  $J_{\text{sense}}$ . The damping constant  $\alpha$  and effective out-of-plane anisotropy field ( $\mu_0 H_{k,\text{out}}$ ) were set to be 0.03 and 0.44 T, respectively, which were obtained experimentally by FM resonance measurements using our W/CoFeB samples. The orientation of spin polarization ( $\boldsymbol{\sigma}$ ) was set along the  $y$  direction to compete with  $H_y$ . We set the duration of STs and  $H_y$  as 120 ns and recorded the time-averaged  $y$  component of magnetization ( $m_{y,\text{avg}}$ ) for the last 40 ns to observe this competing effect. Since both effective fields were proportional to the applied current,  $H_{\text{FL}}/H_{\text{DL}}$  was set at a constant 0.2 for generality and to consider FL-ST.

We first observe that the current-dependent variation of  $m_x$  is limited; therefore, the AMR contribution ( $\propto m_x^2$ ) can be ruled out and reveals that the additional UMR mainly stems from the SMR term ( $\propto 1 - m_x^2$ ). As shown in Fig. 4(a), we swept  $\mu_0 H_{\text{DL}}$  from 0 to 70 mT (corresponding to increasing  $J_{\text{sense}}$  and therefore the DL-ST) to observe the variation of  $m_{y,\text{avg}}$  at different  $\mu_0 H_y$  (with  $\boldsymbol{\sigma}$  opposing  $H_y$ ). The DL-ST from  $\boldsymbol{\sigma}$  that is opposite to the external field competes with  $H_y$  and deviates the magnetization away from the  $y$  direction. With increasing  $\mu_0 H_{\text{DL}}$  from 0 mT to a specific value, the magnetization orientation can be tilted (a jump in  $m_{y,\text{avg}}$ ), which corresponds to the DL-ST switching. This specific value becomes larger as  $\mu_0 H_y$  increases, and we define this threshold value as  $\mu_0 H_{\text{DL,th}}$ . As shown in Fig. 4(b), we plot  $\mu_0 H_{\text{DL,th}}$  as a function of  $\mu_0 H_y$ , and the trend can be well fitted by a linear function with a slope  $H_{\text{DL,th}}/H_y \approx 0.03$ . Assuming that the numerically determined  $H_{\text{DL,th}}$  corresponds to the experimentally determined  $J_{\text{inflection}}$ , we can further estimate the DL-ST efficiency of the W(4)/CoFeB(2) device by [36,37]

$$\xi_{\text{DL}} \approx \frac{2e\mu_0 M_s t_{\text{FM}}}{\hbar} \left( \frac{H_{\text{DL,th}}}{J_{\text{inflection}}} \right) = \frac{2eM_s t_{\text{FM}}}{\hbar} \left( \frac{H_{\text{DL,th}}}{H_y} \frac{J_{\text{inflection}}}{\mu_0 H_y} \right), \quad (2)$$

from which  $|\xi_{\text{DL}}| \approx 0.59$  is determined. Another observable feature is that, in the large  $\mu_0 H_{\text{DL}}$  regime, the saturated  $m_{y,\text{avg}}$  increases as increasing  $H_y$ , which results in a lower SMR contribution ( $\propto 1 - m_{y,\text{avg}}^2$ ). This trend is also consistent with

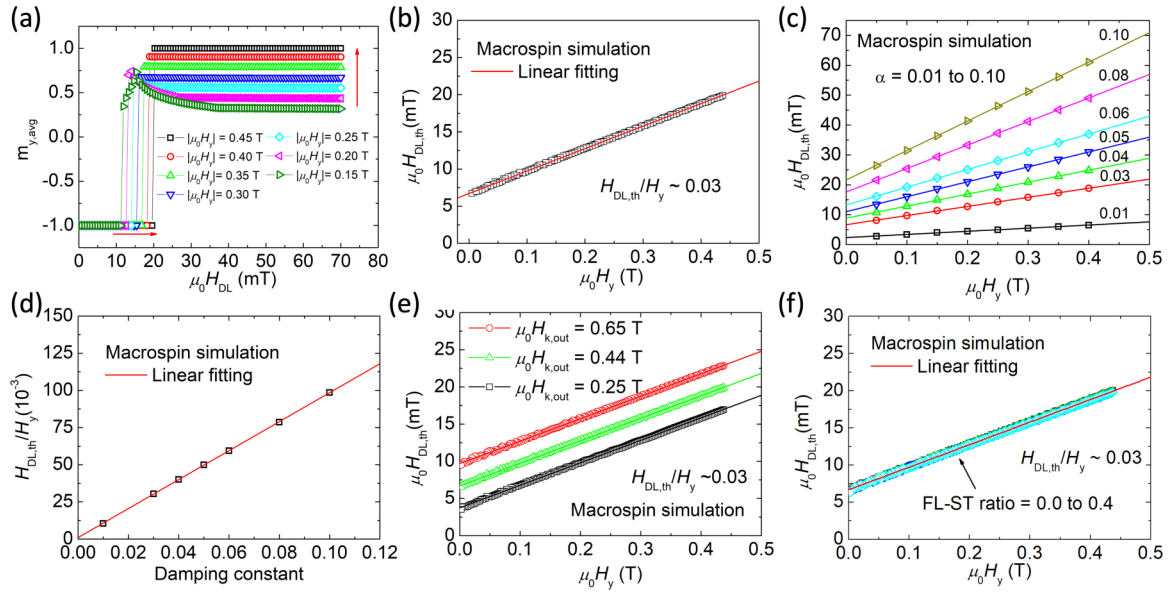


FIG. 4. Macrospin simulation: (a)  $m_{y,\text{avg}}$  as a function of  $\mu_0 H_{\text{DL}} (\propto J_{\text{sense}})$  with different  $\mu_0 H_y$ . The red arrows represent the variation of  $\mu_0 H_{\text{DL,th}}$  and  $m_{y,\text{avg}}$  with increasing  $H_y$ . (b)  $\mu_0 H_y$  dependence of  $\mu_0 H_{\text{DL,th}}$  with fieldlike spin torque (FL-ST)/dampinglike spin torque (DL-ST) ratio = 0.2. (c)  $\mu_0 H_y$  dependence of  $\mu_0 H_{\text{DL,th}}$  with damping constant  $\alpha = 0.01-0.10$ . (d) The summary of slope  $H_{\text{DL,th}}/H_y$  vs damping constant, which are extracted from (a). (e)  $\mu_0 H_y$  dependence of  $\mu_0 H_{\text{DL,th}}$  with  $\mu_0 H_{k,\text{out}} = 0.25, 0.44$ , and  $0.65$  T. (f)  $\mu_0 H_y$  dependence of  $\mu_0 H_{\text{DL,th}}$  with FL-ST/DL-ST ratio = 0.0-0.4. The results for various FL-ST/DL-ST ratios are almost overlapped with each other.

the experimental observation of a lower saturated UMR under a larger  $H_y$ , as shown in Fig. 3(b).

To see how different factors could affect the simulation and thereby the efficiency estimation result, we performed additional macrospin simulations by varying parameters that can influence ST-driven magnetization switching, such as damping constant  $\alpha$ , anisotropy field  $\mu_0 H_{k,\text{out}}$ , and FL-ST/DL-ST ratios. As shown in Figs. 4(c) and 4(d), different magnitudes of  $\alpha$  can affect the slope  $H_{\text{DL,th}}/H_y$ , which increases linearly to  $\alpha$ . This suggests that an accurate determination of  $\alpha$  experimentally is important for using this protocol to estimate  $\xi_{\text{DL}}$ . We also extracted  $H_{\text{DL,th}}/H_y$  with various  $\mu_0 H_{k,\text{out}}$  and FL-ST/DL-ST ratios, which show almost the same slope [Figs. 4(e) and 4(f)], suggesting that the magnitude of  $\mu_0 H_{k,\text{out}}$  and the existence of FL-ST play minor roles in affecting the estimation. In short, the value of  $\alpha$  influences the result of the estimated  $\xi_{\text{DL}}$  in this method, while the variation of  $\mu_0 H_{k,\text{out}}$  and FL-ST does not.

We further performed micromagnetic simulations via UBERMAG [38] (the calculation kernel is based on OOMMF [39]) and MUMAX3 [40] to see if the geometry of the simulated device could affect the estimation. In both UBERMAG and MUMAX3 simulations, the device geometry was set as  $100 \times 100 \times 2$  nm, which was split into 400 cells with dimensions of  $5 \times 5 \times 2$  nm. Note that this is much smaller than the actual device for our experimental tests. To consider exchange and Dzyaloshinskii-Moriya interactions (DMIs) into  $\mathbf{H}_{\text{eff}}$ , the exchange stiffness constant and the interfacial DMI was set as  $1.6 \times 10^{-11}$  J/m and  $2 \times 10^{-4}$  J/m<sup>2</sup>, respectively. The strength of  $\xi_{\text{DL}}$  was set as 0.5 for simplicity. Other parameters were set to be the same as the macrospin simulations. The simulated critical current density  $J_{\text{infection}}$  is defined as the threshold

current density to tilt the magnetization orientation by ST, which has the same physical meaning as the abovementioned  $\mu_0 H_{\text{DL,th}}$ . The  $\mu_0 H_y$  dependence of  $J_{\text{infection}}$  exhibits the same linear trend as found in experiments and macrospin simulations. The slope  $J_{\text{infection}}/\mu_0 H_y \approx 2.20 \times 10^{11}$  A/(m<sup>2</sup>T), is fairly consistent with the experimental results shown in Fig. 3(c).

## VI. ESTIMATION OF THE DL-ST EFFICIENCIES

The protocol mentioned above allows us to systematically determine  $\xi_{\text{DL}}$  from a series of  $W(t_w)/\text{CoFeB}(2)$  devices. As shown in Fig. 5(a),  $J_{\text{infection}}/\mu_0 H_y$  decreases from  $2.33 \times 10^{11}$  A/(m<sup>2</sup>T) at  $t_w = 2$  nm to  $2.14 \times 10^{11}$  A/(m<sup>2</sup>T) at  $t_w = 4$  nm, and then increases to  $2.54 \times 10^{11}$  A/(m<sup>2</sup>T) at  $t_w = 7$  nm. By employing  $J_{\text{infection}}/\mu_0 H_y$  (from experiments) and  $H_{\text{DL,th}}/H_y$  (from simulations) data, the thickness dependence of  $\xi_{\text{DL}}$  is estimated by Eq. (2) and summarized in Fig. 5(b). Here,  $|\xi_{\text{DL}}|$  reaches  $\sim 0.59$  at  $t_w = 4$  nm and then proceeds to decrease as  $W$  thickness increases. This phase transition behavior of  $\xi_{\text{DL}}$  in the  $W/\text{CoFeB}$  heterostructures is fairly consistent with previous reports [22,32,33]. However, since the size of our sample is in the micrometer regime and the proposed estimation protocol is mainly related to the switching process under  $H_y$  and ST, some uncertainties in estimation of  $\xi_{\text{DL}}$  may arise due to the oversimplified macrospin model. This might lead to an overestimation in  $\xi_{\text{DL}}$  since the switching behavior in larger-sized samples typically involves multidomain nucleation, therefore could deviate from the macrospin or single domain prediction [41]. We believe that a more accurate efficiency estimation can be achieved either by shrinking the size of the tested device or by performing micromagnetic simulations using a larger device size.

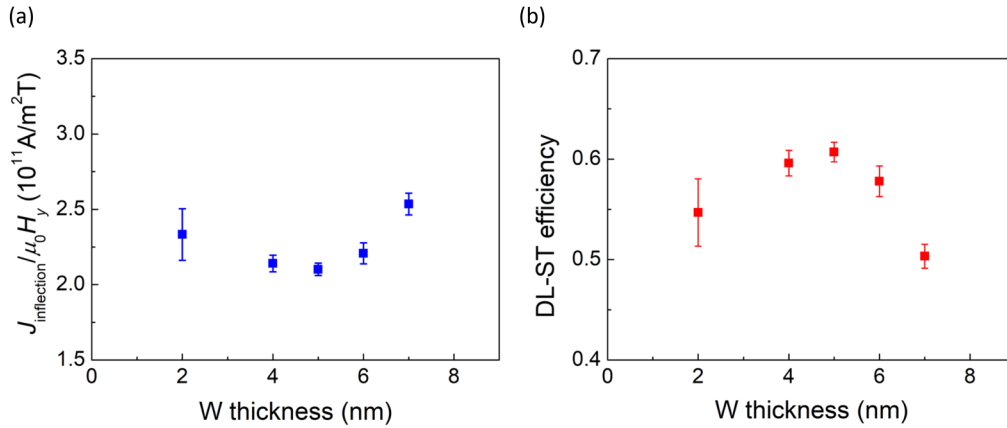


FIG. 5. (a) Experimentally obtained  $J_{\text{inflection}}/\mu_0 H_y$  and (b) the estimated dampinglike spin torque (DL-ST) efficiencies  $|\xi_{\text{DL}}|$  of  $W(t_w)/\text{CoFeB}(2)$  samples as functions of W thickness.

## VII. CONCLUSIONS

To conclude, through systematic current- and field-dependent UMR measurements, we discovered an additional ST-induced UMR (STT-UMR) at the high current regime, which leads to a large UMR ratio of  $\sim 0.36\%$  at room temperature for  $W/\text{CoFeB}$  magnetic heterostructures. This STT-UMR can be attributed to an extra contribution from SMR, which originates from the tilting of magnetization  $\mathbf{M}$  caused by the competition between the DL-ST effective field  $H_{\text{DL}}$  and the applied external field  $H_y$ . This is confirmed by both macrospin and micromagnetic simulations, from which the numerically determined  $H_{\text{DL,th}}/H_y$  can be employed to estimate  $\xi_{\text{DL}}$  to-

gether with the experimentally obtained  $J_{\text{inflection}}/\mu_0 H_y$ . Our studies thus confirm the correlation between the SHE-induced ST and the large room-temperature UMR, thereby providing an alternative approach to characterize DL-ST efficiency.

## ACKNOWLEDGMENTS

The authors acknowledge support from the Ministry of Science and Technology of Taiwan (MOST) under Grant No. MOST-110-2636-M-002-013. This paper is also partly supported by Taiwan Semiconductor Manufacturing Company (TSMC).

- 
- [1] M. N. Baibich, J. M. Broto, A. Fert, F. N. Van Dau, F. Petroff, P. Etienne, G. Creuzet, A. Friederich, and J. Chazelas, Giant Magnetoresistance of (001)Fe/(001)Cr Magnetic Superlattices, *Phys. Rev. Lett.* **61**, 2472 (1988).
- [2] G. Binasch, P. Grünberg, F. Saurenbach, and W. Zinn, Enhanced magnetoresistance in layered magnetic structures with antiferromagnetic interlayer exchange, *Phys. Rev. B* **39**, 4828 (1989).
- [3] R. E. Camley and J. Barnaś, Theory of Giant Magnetoresistance Effects in Magnetic Layered Structures with Antiferromagnetic Coupling, *Phys. Rev. Lett.* **63**, 664 (1989).
- [4] D. D. Djayaprawira, K. Tsunekawa, M. Nagai, H. Maehara, S. Yamagata, N. Watanabe, S. Yuasa, Y. Suzuki, and K. Ando, 230% room-temperature magnetoresistance in CoFeB/MgO/CoFeB magnetic tunnel junctions, *Appl. Phys. Lett.* **86**, 092502 (2005).
- [5] J. Hayakawa, S. Ikeda, Y. M. Lee, F. Matsukura, and H. Ohno, Effect of high annealing temperature on giant tunnel magnetoresistance ratio of CoFeB/MgO/CoFeB magnetic tunnel junctions, *Appl. Phys. Lett.* **89**, 232510 (2006).
- [6] S. Ikeda, J. Hayakawa, Y. Ashizawa, Y. Lee, K. Miura, H. Hasegawa, M. Tsunoda, F. Matsukura, and H. Ohno, Tunnel magnetoresistance of 604% at 300 K by suppression of Ta diffusion in CoFeB/MgO/CoFeB pseudo-spin-valves annealed at high temperature, *Appl. Phys. Lett.* **93**, 082508 (2008).
- [7] M. I. Dyakonov and V. Perel, Current-induced spin orientation of electrons in semiconductors, *Phys. Lett. A* **35**, 459 (1971).
- [8] J. E. Hirsch, Spin Hall Effect, *Phys. Rev. Lett.* **83**, 1834 (1999).
- [9] S. Zhang, Spin Hall Effect in the Presence of Spin Diffusion, *Phys. Rev. Lett.* **85**, 393 (2000).
- [10] H. Nakayama, M. Althammer, Y. T. Chen, K. Uchida, Y. Kajiwara, D. Kikuchi, T. Ohtani, S. Geprags, M. Opel, S. Takahashi, R. Gross, G. E. Bauer, S. T. Goennenwein, and E. Saitoh, Spin Hall Magnetoresistance Induced by a Nonequilibrium Proximity Effect, *Phys. Rev. Lett.* **110**, 206601 (2013).
- [11] S. Cho, S.-h. C. Baek, K.-D. Lee, Y. Jo, and B.-G. Park, Large spin Hall magnetoresistance and its correlation to the spin-orbit torque in W/CoFeB/MgO structures, *Sci. Rep.* **5**, 14668 (2015).
- [12] J. Kim, P. Sheng, S. Takahashi, S. Mitani, and M. Hayashi, Spin Hall Magnetoresistance in Metallic Bilayers, *Phys. Rev. Lett.* **116**, 097201 (2016).
- [13] C. O. Avci, K. Garello, A. Ghosh, M. Gabureac, S. F. Alvarado, and P. Gambardella, Unidirectional spin Hall magnetoresistance in ferromagnet/normal metal bilayers, *Nat. Phys.* **11**, 570 (2015).
- [14] C. O. Avci, K. Garello, J. Mendil, A. Ghosh, N. Blazakis, M. Gabureac, M. Trassin, M. Fiebig, and P. Gambardella, Magnetoresistance of heavy and light metal/ferromagnet bilayers, *Appl. Phys. Lett.* **107**, 192405 (2015).

- [15] Y. Yin, D.-S. Han, M. C. de Jong, R. Lavrijsen, R. A. Duine, H. J. Swagten, and B. Koopmans, Thickness dependence of unidirectional spin-hall magnetoresistance in metallic bilayers, *Appl. Phys. Lett.* **111**, 232405 (2017).
- [16] C. O. Avci, J. Mendil, G. S. Beach, and P. Gambardella, Origins of the unidirectional spin Hall magnetoresistance in metallic bilayers, *Phys. Rev. Lett.* **121**, 087207 (2018).
- [17] Y.-T. Chen, S. Takahashi, H. Nakayama, M. Althammer, S. T. B. Goennenwein, E. Saitoh, and G. E. W. Bauer, Theory of spin Hall magnetoresistance, *Phys. Rev. B* **87**, 144411 (2013).
- [18] K. Yasuda, A. Tsukazaki, R. Yoshimi, K. S. Takahashi, M. Kawasaki, and Y. Tokura, Large Unidirectional Magnetoresistance in a Magnetic Topological Insulator, *Phys. Rev. Lett.* **117**, 127202 (2016).
- [19] T. Li, S. Kim, S.-J. Lee, S.-W. Lee, T. Koyama, D. Chiba, T. Moriyama, K.-J. Lee, K.-J. Kim, and T. Ono, Origin of threshold current density for asymmetric magnetoresistance in Pt/Py bilayers, *Appl. Phys. Express* **10**, 073001 (2017).
- [20] I. Borisenko, V. Demidov, S. Urazhdin, A. Rinkevich, and S. Demokritov, Relation between unidirectional spin Hall magnetoresistance and spin current-driven magnon generation, *Appl. Phys. Lett.* **113**, 062403 (2018).
- [21] K.-J. Kim, T. Li, S. Kim, T. Moriyama, T. Koyama, D. Chiba, K.-J. Lee, H.-W. Lee, and T. Ono, Possible contribution of high-energy magnons to unidirectional magnetoresistance in metallic bilayers, *Appl. Phys. Express* **12**, 063001 (2019).
- [22] J. Liu, T. Ohkubo, S. Mitani, K. Hono, and M. Hayashi, Correlation between the spin Hall angle and the structural phases of early  $5d$  transition metals, *Appl. Phys. Lett.* **107**, 232408 (2015).
- [23] Y.-H. Wang, W.-C. Chen, S.-Y. Yang, K.-H. Shen, C. Park, M.-J. Kao, and M.-J. Tsai, Interfacial and annealing effects on magnetic properties of CoFeB thin films, *J. Appl. Phys.* **99**, 08M307 (2006).
- [24] Y.-T. Liu, T.-Y. Chen, T.-H. Lo, T.-Y. Tsai, S.-Y. Yang, Y.-J. Chang, J.-H. Wei, and C.-F. Pai, Determination of Spin-Orbit-Torque Efficiencies in Heterostructures with In-Plane Magnetic Anisotropy, *Phys. Rev. Appl.* **13**, 044032 (2020).
- [25] K. Olejník, V. Novák, J. Wunderlich, and T. Jungwirth, Electrical detection of magnetization reversal without auxiliary magnets, *Phys. Rev. B* **91**, 180402(R) (2015).
- [26] N. H. Duy Khang and P. N. Hai, Giant unidirectional spin Hall magnetoresistance in topological insulator-ferromagnetic semiconductor heterostructures, *J. Appl. Phys.* **126**, 233903 (2019).
- [27] B. Raquet, M. Viret, E. Sondergard, O. Cespedes, and R. Mamy, Electron-magnon scattering and magnetic resistivity in  $3d$  ferromagnets, *Phys. Rev. B* **66**, 024433 (2002).
- [28] A. P. Mihai, J. P. Attané, A. Marty, P. Warin, and Y. Samson, Electron-magnon diffusion and magnetization reversal detection in FePt thin films, *Phys. Rev. B* **77**, 060401(R) (2008).
- [29] V. E. Demidov, S. Urazhdin, E. R. J. Edwards, M. D. Stiles, R. D. McMichael, and S. O. Demokritov, Control of Magnetic Fluctuations by Spin Current, *Phys. Rev. Lett.* **107**, 107204 (2011).
- [30] S. Langenfeld, V. Tshitoyan, Z. Fang, A. Wells, T. Moore, and A. Ferguson, Exchange magnon induced resistance asymmetry in permalloy spin-Hall oscillators, *Appl. Phys. Lett.* **108**, 192402 (2016).
- [31] C.-F. Pai, L. Liu, Y. Li, H. Tseng, D. Ralph, and R. Buhrman, Spin transfer torque devices utilizing the giant spin Hall effect of tungsten, *Appl. Phys. Lett.* **101**, 122404 (2012).
- [32] S. Mondal, S. Choudhury, N. Jha, A. Ganguly, J. Sinha, and A. Barman, All-optical detection of the spin Hall angle in W/CoFeB/SiO<sub>2</sub> heterostructures with varying thickness of the tungsten layer, *Phys. Rev. B* **96**, 054414 (2017).
- [33] T.-C. Wang, T.-Y. Chen, C.-T. Wu, H.-W. Yen, and C.-F. Pai, Comparative study on spin-orbit torque efficiencies from W/ferromagnetic and W/ferrimagnetic heterostructures, *Phys. Rev. Mater.* **2**, 014403 (2018).
- [34] L. Zhu and R. A. Buhrman, Maximizing Spin-Orbit-Torque Efficiency of Pt/Ti Multilayers: Trade-Off Between Intrinsic Spin Hall Conductivity and Carrier Lifetime, *Phys. Rev. Appl.* **12**, 051002(R) (2019).
- [35] C. O. Avci, K. Garello, M. Gabureac, A. Ghosh, A. Fuhrer, S. F. Alvarado, and P. Gambardella, Interplay of spin-orbit torque and thermoelectric effects in ferromagnet/normal-metal bilayers, *Phys. Rev. B* **90**, 224427 (2014).
- [36] J. Z. Sun, Spin-current interaction with a monodomain magnetic body: a model study, *Phys. Rev. B* **62**, 570 (2000).
- [37] R. H. Koch, J. A. Katine, and J. Z. Sun, Time-Resolved Reversal of Spin-Transfer Switching in a Nanomagnet, *Phys. Rev. Lett.* **92**, 088302 (2004).
- [38] M. Beg, R. A. Pepper, and H. Fangohr, User interfaces for computational science: a domain specific language for OOMMF embedded in Python, *AIP Adv.* **7**, 056025 (2017).
- [39] M. J. Donahue and D. G. Porter, *OOMMF User's Guide Version 1.0*, (National Institute of Standards and Technology, Gaithersburg, 1999), <http://math.nist.gov/oommf/>.
- [40] A. Vansteenkiste, J. Leliaert, M. Dvornik, M. Helsen, F. Garcia-Sanchez, and B. Van Waeyenberge, The design and verification of MUMAX3, *AIP Adv.* **4**, 107133 (2014).
- [41] L. Zhu, D. C. Ralph, and R. A. Buhrman, Lack of Simple Correlation between Switching Current Density and Spin-Orbit-Torque Efficiency of Perpendicularly Magnetized Spin-Current-Generator-Ferromagnet Heterostructures, *Phys. Rev. Appl.* **15**, 024059 (2021).